

# Solar Neutrinos with Magnetic Moment and Solar Field Profiles

João Pulido \*

*Centro de Física das Interações Fundamentais (CFIF)  
Departamento de Física, Instituto Superior Técnico  
Av. Rovisco Pais, P-1049-001 Lisboa, Portugal*

## Abstract

A statistical analysis of the pre-SNO solar neutrino data is made assuming the solar neutrino deficit to be resolved by the interaction of the neutrino magnetic moment with the solar magnetic field. Given the general characteristics of the field profiles known to lead to the best event rate predictions, several specific choices of profiles are assumed and fits to the rates, to the electron recoil spectrum in SuperKamiokande and to the combined rates and spectrum are performed. Both the rate and spectrum fits are remarkably better than in a previous analysis of the magnetic moment solution which used a former standard solar model and previous data, and in particular, rate fits are far better than those from oscillations. The global analysis also reflects the general very good quality of the fits.

---

\*E-mail: pulido@beta.ist.utl.pt

Whereas the apparent anticorrelation of the neutrino event rate with sunspot activity claimed long ago by the Homestake collaboration [1] remained unconfirmed by other experiments [2], [3], [4] and theoretical analyses [5], the magnetic moment solution to the solar neutrino problem is at present an important possibility to be explored in the quest for an explanation of the solar neutrino deficit. This is the idea, originally proposed by Cisneros [6], and later revived by Voloshin, Vysotsky and Okun [7], that a large magnetic moment of the neutrino may interact with the magnetic field of the sun, converting weakly active to sterile neutrinos. It now appears in fact that this deficit is energy dependent, in the sense that neutrinos of different energies are suppressed differently. In order to provide an energy dependent deficit, the conversion mechanism from active to nonactive neutrinos must be resonant, with the location of the critical density being determined by the neutrino energy. Thus was developed the idea of the resonant spin flavour precession (RSFP) proposed in 1988 [8]. It involves the simultaneous flip of both chirality and flavour consisting basically in the assumption that the neutrino conversion due to magnetic moment and magnetic field takes place through a resonance inside matter in much the same way as matter oscillations [9]. A sunspot activity related event rate in a particular experiment would hence imply that most of the neutrinos with energies relevant to that experiment have their resonances in the sunspot range. However, the depth of sunspots is unknown (they may not extend deeper than a few hundred kilometers) and the observed field intensity is too small in sunspots to allow for a significant conversion. The anticorrelation argument has therefore lost its appeal for several years now.

Despite the absence of the anticorrelation argument, several main reasons may be invoked to motivate RSFP and investigating its consequences for solar neutrinos. In fact both RSFP and all oscillation scenarios indicate a drop in the survival probability from the low energy (pp) to the intermediate energy neutrino sector ( $^7\text{Be}$ , CNO, pep) and a subsequent moderate rise as the energy increases further into the  $^8\text{B}$  sector. The magnetic field profiles providing good fits to the event rates from solar neutrino experiments typically show the characteristic of a sharp rise in intensity at some point in the solar interior, followed by a progressive moderate decrease [10], [11]. This is in opposite correspondence with the energy dependence of the probability in the sense that the strongest field intensities correspond to the smallest survival probabilities. Hence RSFP offers a unique explanation for the general shape of the probability, which naturally appears as a consequence of the field profile. On the other hand, from solar physics and helioseismology such a sharp rise and peak field intensity is expected to occur along the tachocline, the region extending from the upper radiative zone to the lower convective zone, where the gradient of the angular velocity of solar matter is different from zero [12], [13]. Furthermore, it has become clear [14], [10], [11] that RSFP provides event rate fits from the solar neutrino experiments that are far better than all oscillation ones [15], [16]. Finally, there are recent claims in the literature for evidence of a neutrino flux histogram [17] containing two peaks, an indication of variability pointing towards a nonzero magnetic moment of the neutrino.

The aim of this paper is to present a statistical analysis of seven field profiles proposed in

[10], all obeying the general features described above, in the light of the updated standard solar model (BP 2000) [18] and the most recent data [1, 2, 3, 4]. For each profile the best fits of both the rate and recoil electron spectrum in neutrino electron scattering are determined along with the corresponding  $\chi^2$ . Unlike a previous analysis, the contribution of hep neutrinos is taken into account in the spectrum fits. The results show a remarkable improvement in the quality of both sets of fits with respect to ref. [10] where the BP'98 standard solar model [19] and the available data at the time were used. Throughout the calculations a value of  $\mu_\nu = 10^{-11}\mu_B$  is assumed.

The profiles investigated are the following:

*Profiles (1), (2)*

$$B = 0 \quad , \quad x < x_R \quad (1)$$

$$B = B_0 \frac{x - x_R}{x_C - x_R} \quad , \quad x_R \leq x \leq x_C \quad (2)$$

$$B = B_0 \left[ 1 - \frac{x - x_C}{1 - x_C} \right] \quad , \quad x_C \leq x \leq 1 \quad (3)$$

where  $x$  is the fraction of the solar radius and units are in Gauss. For profile 1  $x_R = 0.70$ ,  $x_C = 0.85$  and for profile (2)  $x_R = 0.65$ ,  $x_C = 0.80$ .

*Profile (3)*

$$B = 0 \quad , \quad x < x_R \quad (4)$$

$$B = B_0 \frac{x - x_R}{x_C - x_R} \quad , \quad x_R \leq x \leq x_C \quad (5)$$

$$B = B_0 \left[ 1 - \left( \frac{x - 0.7}{0.3} \right)^2 \right] \quad , \quad x_C < x \leq 1 \quad (6)$$

with  $x_R = 0.65$ ,  $x_C = 0.75$ .

*Profile (4)*

$$B = 0 \quad , \quad x < x_R \quad (7)$$

$$B = B_0 \left[ 1 - \left( \frac{x - 0.7}{0.3} \right)^2 \right] \quad , \quad x \geq x_R, \quad (8)$$

with  $x_R = 0.71$ .

*Profile (5)*

$$B = 0 \quad , \quad x < x_R \quad (9)$$

$$B = \frac{B_0}{\cosh 30(x - x_R)} \quad , \quad x \geq x_R \quad (10)$$

with  $x_R = 0.71$ .

*Profile (6)*

$$B = 2.16 \times 10^3 \quad , \quad x \leq 0.7105 \quad (11)$$

$$B = B_1 \left[ 1 - \left( \frac{x - 0.75}{0.04} \right)^2 \right], \quad 0.7105 < x < 0.7483 \quad (12)$$

$$B = \frac{B_0}{\cosh 30(x - 0.7483)}, \quad 0.7483 \leq x \leq 1 \quad (13)$$

with  $B_0 = 0.998B_1$ .

*Profile (7)*

$$B = 2.16 \times 10^3, \quad x \leq 0.7105 \quad (14)$$

$$B = B_0 \left[ 1 - \left( \frac{x - 0.75}{0.04} \right)^2 \right], \quad 0.7105 < x < 0.7483 \quad (15)$$

$$B = 1.1494B_0[1 - 3.4412(x - 0.71)], \quad 0.7483 \leq x \leq 1. \quad (16)$$

The ratios of the RSFP to the SSM event rates  $R_{Ga,Cl,SK}^{th}$  are defined as before [10] with the exception of the SuperKamiokande one in which the energy resolution function [20] is now taken into account

$$R_{SK}^{th} = \frac{\sum_i \int_0^\infty dE_e \int_{E'_{em}}^{E'_{eM}} dE'_e f(E'_e, E_e) \int_{E_m}^{E_M} dE \phi_i(E) [P(E) \frac{d\sigma_W}{dT'} + (1 - P(E)) \frac{d\sigma_{\bar{W}}}{dT'}]}{\sum_i \int_0^\infty dE_e \int_{E'_{em}}^{E'_{eM}} dE'_e f(E'_e, E_e) \int_{E_m}^{E_M} dE \phi_i(E) \frac{d\sigma_W}{dT'}} \quad (17)$$

Here  $\phi_i(E)$  is the neutrino flux for component  $i$  ( $i = hep, {}^8B$ ) and  $f(E'_e, E_e)$  is the energy resolution function of the detector in terms of the physical ( $E'_e$ ) and the measured ( $E_e$ ) electron energy ( $E_e = T + m_e$ ). The lower limit of  $E'_e$  is the detector threshold energy ( $E'_{em} = E_{eth}$  with  $E_{eth} = 5.5\text{MeV}$ ) and the upper limit is evaluated from the maximum neutrino energy  $E_M$  [10]

$$T'_M = \frac{2E_M^2}{m_e + 2E_M}. \quad (18)$$

For the lower [10] and upper [21] integration limits of the neutrino energy one has respectively

$$E_m = \frac{T' + \sqrt{T'^2 + 2m_e T'}}{2}, \quad E_M = 15\text{MeV} \quad (i = {}^8B), \quad E_M = 18.8\text{MeV} \quad (i = hep). \quad (19)$$

The weak differential cross sections appearing in equation (17) are given by

$$\frac{d\sigma_W}{dT} = \frac{G_F^2 m_e}{2\pi} [(g_V + g_A)^2 + (g_V - g_A)^2 \left(1 - \frac{T}{E}\right)^2 - (g_V^2 - g_A^2) \frac{m_e T}{E^2}] \quad (20)$$

for  $\nu_e e$  scattering, with  $g_V = \frac{1}{2} + 2\sin^2\theta_W$ ,  $g_A = \frac{1}{2}$ . For  $\bar{\nu}_\mu e$  and  $\bar{\nu}_\tau e$  scattering,

$$\frac{d\sigma_{\bar{W}}}{dT} = \frac{G_F^2 m_e}{2\pi} [(g_V - g_A)^2 + (g_V + g_A)^2 \left(1 - \frac{T}{E}\right)^2 - (g_V^2 - g_A^2) \frac{m_e T}{E^2}] \quad (21)$$

with  $g_V = -\frac{1}{2} + 2\sin^2\theta_W$ ,  $g_A = -\frac{1}{2}$ .

The recoil electron spectrum in SuperKamiokande is now defined as

$$R_{SK}^{th} = \frac{\sum_i \int_{E_{ej}}^{E_{ej+1}} dE_e \int_{E'_{em}}^{E'_{eM}} dE'_e f(E'_e, E_e) \int_{E_m}^{E_M} dE \phi_i(E) [P(E) \frac{d\sigma_W}{dT'} + (1 - P(E)) \frac{d\sigma_W}{dT'}]}{\sum_i \int_{E_{ej}}^{E_{ej+1}} dE_e \int_{E'_{em}}^{E'_{eM}} dE'_e f(E'_e, E_e) \int_{E_m}^{E_M} dE \phi_i(E) \frac{d\sigma_W}{dT'}} \quad (22)$$

with  $i = hep$ ,  $^8B$  for 18 energy bins ( $j=1, \dots, 18$ ) [2].

The fluxes and partial event rates for each neutrino component in each experiment were taken from [18] and the solar neutrino spectra from Bahcall's homepage [21]. The contribution of the hep flux to both the Gallium and Homestake event rates was neglected. The  $\chi^2$  analysis for the ratios of event rates and electron spectrum in SuperKamiokande was done following the standard procedure described in [10]<sup>†</sup>.

The ratios of event rates to the SSM event rates and the recoil electron spectrum normalized to the SSM one, both denoted by  $R^{th}$  in the following, were calculated in the parameter ranges  $\Delta m_{21}^2 = (4 - 22) \times 10^{-9} eV^2$ ,  $B_0 = (3 - 30) \times 10^4 G$  for all magnetic field profiles and inserted in the  $\chi^2$  definitions for the rates and spectrum,

$$\chi_{rates}^2 = \sum_{j_1, j_2=1}^3 (R_{j_1}^{th} - R_{j_1}^{exp}) [\sigma_{rates}^2(tot)]_{j_1 j_2}^{-1} (R_{j_2}^{th} - R_{j_2}^{exp}) \quad (23)$$

with (Ga=1, Cl=2, SK=3)

$$\chi_{sp}^2 = \sum_{j_1, j_2=1}^{18} (R_{j_1}^{th} - R_{j_1}^{exp}) [\sigma_{sp}^2(tot)]_{j_1 j_2}^{-1} (R_{j_2}^{th} - R_{j_2}^{exp}). \quad (24)$$

The quantities  $R^{exp}$  in eqs. (21), (22) are directly read from tables I, II respectively and the total error matrices  $\sigma^2(tot)$  are derived from the definitions given in [10], using [21] and the error bars in tables I, II. In fitting the rates one has 3 experiments and 2 parameters (the mass square difference between neutrino flavours and the value of the field at the peak), hence the number of degrees of freedom is one, while for the spectrum there are 18 data points, hence 16 degrees of freedom. For global fits one has

$$\chi_{gl}^2 = \sum_{j_1, j_2=1}^{21} (R_{j_1}^{th} - R_{j_1}^{exp}) [\sigma_{gl}^2(tot)]_{j_1 j_2}^{-1} (R_{j_2}^{th} - R_{j_2}^{exp}). \quad (25)$$

Here index values 1, 2, 3 are used for the rates and 4, ..., 21 for the spectrum. The best fits for the rates in terms of  $\Delta m_{21}^2$ ,  $B_0$  and the corresponding values of  $\chi^2$  for rates, spectrum and global fits are shown in table III. In table IV the spectrum best fits are shown with

---

<sup>†</sup>Here only the main definitions and differences are registered. For the calculational details we refer the reader to ref.[10].

the corresponding values of  $\chi_{sp_{min}}^2$  and table V shows the global best fits with the values of  $\chi_{rates}^2$ ,  $\chi_{sp}^2$  in each profile. In this case the number of d.o.f. is 19 (=21-2).

It is seen that the rate fits (table III) are in some cases excellent, with four of the profiles being much favoured, in particular profile 2. The most unfavoured ones (profiles 4, 5 and 7) give nevertheless substantially smaller  $\chi^2$  as compared to oscillations [15, 16]. It is difficult at present to develop a general distinction between the characteristics of those profiles which provide the best fits and the others. In profiles 6 and 7 for instance the field intensity along the bottom of the convective zone rises in the same way and the quality of the rate fits is quite different: this suggests that an upward facing concavity (profile 6) along the upper convective zone is preferred relative to a constant slope (profile 7). In fact, since the low energy sector of the  ${}^8B$  neutrinos is highly suppressed because their resonances are located close to the intermediate energy ones (*pep*, *CNO*) whose suppression has to be maximal, the higher energy sector of  ${}^8B$  has to undergo little suppression in order to ensure a survival probability close to 1/2 as reported by SuperKamiokande. Hence the magnetic field should decrease steeply at first after its maximum and then more smoothly. The same conclusion is also suggested from inspection of profiles 4 and 5: while they exhibit a sudden rise at the bottom of the convective zone with infinite slope, their downward slopes have opposite shapes to each other, favouring the case with an upward facing concavity (profile 5). As for profile 4 the fits still worsen, as expected, if the exponent 2 in eq. (8) is increased. An infinite rise in field intensity (profiles 4 and 5) is also disfavoured relative to a finite one (compare 3 with 4 and 6 with 5). The case of the two triangle profiles (1 and 2) suggests that the upward slope should be higher than the downward one.

Table III shows unusually large values of  $\chi_{gl}^2$  at the rate best fits for profiles 4 and 7. This is related to a high instability of  $\chi^2$  both for rates and global fits against small variations of  $\Delta m_{21}^2$  and  $B_0$  not shared by other profiles, as can be seen from a comparison with table V.

The 90 and 99% CL regions for the rates defined in the  $\Delta m_{21}^2, B_0$  plane from the condition  $\chi^2 \leq \chi_{min}^2 + \Delta\chi^2$  with, for one degree of freedom,  $\Delta\chi^2 = 2.71$  and 6.64 respectively, are shown in fig.1. The four profiles chosen are those for which  $\chi_{min}^2 < 0.1$ . As far as the spectrum fits are concerned, the results for the minima of  $\chi_{sp}^2$  are also remarkably good (see table IV). A comparison of tables III and IV and inspection of fig.1 show a discrepancy between the rate and spectrum best fits. To further examine this discrepancy one can analyse for each profile the difference between the CL's corresponding to  $\chi_{sp}^2$  at the rate and spectrum best fits also listed in table IV [22]. For 16 d.o.f. it is seen from the values of this difference that all rate best fits lie within a region of 10.5% CL with respect to the spectrum best fit: the function  $\chi_{sp}^2$  has a weak dependence on the parameters  $B_0$  and  $\Delta m_{21}^2$ , so that the mismatch between the rates and spectrum fits is statistically meaningless. Hence one should expect very good global fits. In fact the global best fits, all with a remarkably low  $\chi_{global}^2$  (see table V) always lie within a similar (11.4% CL) region relative to the spectrum ones and also very close to the rate best fits, namely within a 41% CL region with respect to these, as can be derived from tables III, IV and V and using ref. [22].

As an example, the predicted spectrum (eq. (22)) for profile 1 is shown in figs.2 and 3 respectively at the rate and spectrum best fits superimposed on the SuperKamiokande data. The moderate rise occurring for  $E_e \geq 12\text{MeV}$  is the effect of hep neutrinos.

As previously referred, a value of  $\mu_\nu = 10^{-11}\mu_B$  was assumed in the calculations. Since the order parameter is the product  $\mu B$  and the peak value of the field is probably as large as  $3 \times 10^5 G$  [12, 13], the best fits imply an effective value of  $\mu_\nu$  in the range  $(2 - 5) \times 10^{-12}\mu_B$  in consistency with most astrophysical bounds [23].

To summarize, the analysis of prospects for the magnetic moment solution to the solar neutrino problem made on the basis of BP'2000 solar standard model and using the most recent pre-SNO data reveals extremely good fits for the rates for a class of field profiles with a steep rise across the bottom of the convective zone and a more moderate decrease up to the surface. There is a substantial and noteworthy improvement in the quality of the fits with respect to a previous analysis using BP'98 [19] and previous data. Spectrum fits are also quite good and consistent with the rate fits.

In the present analysis only time averaged data were considered and a fitting was made to a time constant profile 'buried' in the solar interior. If, on the contrary, the active neutrino flux turns out to be time dependent, a situation most likely to be interpreted through the magnetic moment solution with a time dependent interior field, the present approach is obviously inadequate and all fittings thus made will in some way be flawed. Averaging the event rates over time implies disregarding possible information in the data which otherwise is available if different periods of time are considered [17]. The robustness of such a procedure will greatly improve with the accumulation of more data.

## References

- [1] Homestake Collaboration: B. T. Cleveland *et al.*, *Astrophys. J.* **496**, 505 (1998); B. T. Cleveland *et al.*, *Nucl. Phys. B* (Proc. Suppl.) **38**, 47 (1995); R. Davis, *Prog. Part. Nucl. Phys.* **32**, 13 (1994).
- [2] Y. Suzuki for the SuperKamiokande Collaboration, in *Neutrino 2000*, Proceedings of the 19th International Conference on Neutrino Physics and Astrophysics (Sudbury, Canada, June 2000) to be published. Transparencies available at [www.laurentian.ca/physics/nu2000](http://www.laurentian.ca/physics/nu2000).
- [3] SAGE Collaboration: V. Gavrin, in *Neutrino 2000*.
- [4] Gallex+GNO Collaboration: E. Bellotti, in *Neutrino 2000*.
- [5] G. Walther, *Phys. Rev. Lett.* **79** 4522 (1998).
- [6] A. Cisneros, *Astrophys. Space Sci.* **10** 87 (1971).

- [7] M. B. Voloshin, M. I. Vysotsky, L. B. Okun, Soviet J. of Nucl. Phys. **44** 440 (1986); M. B. Voloshin, M. I. Vysotsky, Soviet J. of Nucl. Phys. **44** 544 (1986).
- [8] C. S. Lim and W. J. Marciano, Phys. Rev. **D37**, 1368 (1988); E. Kh. Akhmedov, Sov. J. Nucl. Phys. **48**, 382 (1988); E. Kh. Akhmedov, Phys. Lett. **B 213**, 64 (1988).
- [9] L. Wolfenstein, Phys. Rev. **D 17**, 2369 (1978); **20**, 2634 (1979); S. P. Mikheyev and A. Smirnov, Sov. J. Nucl. Phys. **42**, 913 (1985).
- [10] J. Pulido, E. Kh. Akhmedov, Astropart. Phys. **13** 227 (2000).
- [11] O. G. Miranda, C. Peña Garay, T. I. Rashba, V. B. Semikoz, J. W. F. Valle, hep-ph/0005259, to be published in Nucl. Phys. **B**.
- [12] E. N. Parker in "The Structure of the Sun", Proc. of the VI Canary Islands School, Ed. Roca Cortes and F. Sanchez, Cambridge University Press 1996 p. 299.
- [13] H. M. Antia, S. M. Chitre, M. J. Thompson, astro-ph/0005587, to be published in Astron. and Astrophys.
- [14] M. Guzzo and H. Nunokawa, Astropart. Phys. **12** 87 (1999), hep-ph/9810408.
- [15] J. N. Bahcall, P. I. Krastev and A. Yu. Smirnov, Phys. Rev. **D 58** 096016 (1998);
- [16] M.C. Gonzalez-Garcia, P.C. de Holanda, C. Pena-Garay and J.W.F. Valle, Nucl. Phys. **B573** 3 (2000), hep-ph/9906469.
- [17] J. Scargle and P. Sturrock, astro-ph/0011228, to be published in Astrophys. J. Lett.
- [18] J. N. Bahcall, M. H. Pinsonneault, S. Basu, astro-ph/0010346.
- [19] J. N. Bahcall, S. Basu, M. H. Pinsonneault, Phys. Lett. **B433** 1 (1998).
- [20] SuperKamiokande Collaboration, Y. Fukuda *et al.*, Phys. Rev. Lett. **81** 1158 (1998); Erratum-*ibid.* **81** 4279 (1998).
- [21] J. N. Bahcall's homepage, <http://www.sns.ias.edu/~jnb/>.
- [22] Review of Particle Properties, D. E. Groom *et al.*, The European Physical Journal **C15** 1 (2000).
- [23] S. I. Blinnikov, Institute for Theoretical and Experimental Physics Report No. ITEP-88-19 (1988), unpublished; S. I. Blinnikov, V.S. Imshennik, D.K. Nadyozhin, Sov. Sci. Rev. **E Astrophys. Space Sci.** **6**, 185 (1987); G.G. Raffelt, Phys. Rev. Lett. **64** (1990) 2856; Astrophys. J. **365** (1990) 559; V. Castellani and S. Degl'Innocenti, Astrophys. J. **402**, 574 (1993).



Experiment	Data	Theory	Data/Theory	Reference
Homestake	$2.56 \pm 0.16 \pm 0.15$	$7.7 \pm_{1.1}^{1.3}$	$0.332 \pm 0.05$	[1]
Ga	$74.7 \pm 5.13$	$129 \pm_6^8$	$0.59 \pm 0.06$	[4],[3]
SuperKamiokande	$2.4 \pm 0.085$	$5.15 \pm_{0.7}^{1.0}$	$0.465 \pm 0.052$	[2]

Table I - Data from the solar neutrino experiments. Units are SNU for Homestake and Gallium and  $10^6 cm^{-2}s^{-1}$  for SuperKamiokande. The result for Gallium is the combined one from SAGE and Gallex+GNO.

Energy bin (MeV)	$R_i^{exp}$
$5.5 < E_e < 6$	$0.461 \pm 0.025$
$6 < E_e < 6.5$	$0.438 \pm 0.02$
$6.5 < E_e < 7$	$0.455 \pm 0.016$
$7 < E_e < 7.5$	$0.474 \pm 0.016$
$7.5 < E_e < 8$	$0.490 \pm 0.018$
$8 < E_e < 8.5$	$0.477 \pm 0.018$
$8.5 < E_e < 9$	$0.455 \pm 0.018$
$9 < E_e < 9.5$	$0.463 \pm 0.021$
$9.5 < E_e < 10$	$0.472 \pm 0.026$
$10 < E_e < 10.5$	$0.460 \pm 0.027$
$10.5 < E_e < 11$	$0.452 \pm 0.027$
$11 < E_e < 11.5$	$0.473 \pm 0.033$
$11.5 < E_e < 12$	$0.457 \pm 0.037$
$12 < E_e < 12.5$	$0.429 \pm 0.041$
$12.5 < E_e < 13$	$0.488 \pm 0.049$
$13 < E_e < 13.5$	$0.493 \pm 0.058$
$13.5 < E_e < 14$	$0.583 \pm 0.062$
$14 < E_e < 20$	$0.505 \pm 0.078$

Table II - Recoil electron energy bins in SuperKamiokande (1117 days) and the corresponding ratio of the experimental to the SSM event rate [2].

Profile	Best fit ( $\Delta m_{21}^2, B_0$ )	$\chi_{rates_{min}}^2/1d.o.f.$	$\chi_{sp}^2/16d.o.f.$	$\chi_{gl}^2/19d.o.f.$
1	$(7.08 \times 10^{-9} eV^2, 6.6 \times 10^4 G)$	$3.71 \times 10^{-2}$	9.85	12.73
2	$(1.25 \times 10^{-8} eV^2, 1.28 \times 10^5 G)$	$9.13 \times 10^{-4}$	11.1	12.82
3	$(1.26 \times 10^{-8} eV^2, 9.5 \times 10^4 G)$	$5.96 \times 10^{-2}$	9.72	13.24
4	$(1.7 \times 10^{-8} eV^2, 1.7 \times 10^5 G)$	0.357	11.45	41.46
5	$(2.1 \times 10^{-8} eV^2, 1.42 \times 10^5 G)$	0.133	11.7	11.93
6	$(1.65 \times 10^{-8} eV^2, 9.7 \times 10^4 G)$	$9.51 \times 10^{-3}$	11.35	14.19
7	$(1.50 \times 10^{-8} eV^2, 2.3 \times 10^5 G)$	0.38	10.94	81.44

Table III - Rate fits: the values of  $\Delta m_{21}^2$  and  $B_0$  at the best fit of the rate for each profile, the value of  $\chi_{rates_{min}}^2$  and the corresponding values of  $\chi_{sp}^2$  and  $\chi_{tot}^2$ .

Profile	Best fit ( $\Delta m_{21}^2, B_0$ )	$\chi_{sp_{min}}^2/16d.o.f.$	$CL(\chi_{sp_{min}}^2) - CL(\chi_{sp_{rates}}^2)$
1	$(3.7 \times 10^{-9} eV^2, 4.3 \times 10^4 G)$	9.46	1.89%
2	$(6.4 \times 10^{-9} eV^2, 1.26 \times 10^5 G)$	9.93	6.70%
3	$(7.7 \times 10^{-9} eV^2, 9.5 \times 10^4 G)$	9.48	1.15%
4	$(\leq 10^{-11} eV^2, 8.66 \times 10^4 G)$	9.74	9.90%
5	$(9 \times 10^{-9} eV^2, 1.43 \times 10^5 G)$	9.94	10.5%
6	$(7.8 \times 10^{-9} eV^2, 9.5 \times 10^4 G)$	10.0	7.93%
7	$(\leq 10^{-11} eV^2, 2.27 \times 10^5 G)$	9.75	6.62%

Table IV - Spectrum fits: the values of  $\Delta m_{21}^2$  and  $B_0$  at the best fit of the spectrum for each profile, the corresponding value of  $\chi_{sp_{min}}^2$  and the difference between the confidence levels (or goodness of fits) of the spectrum and the rate best fits for 16 d.o.f.(see the main text for details). For profiles 4 and 7  $\chi_{sp_{min}}^2$  is an asymptotic value for small  $\Delta m_{21}^2$ .

Profile	Best fit ( $\Delta m_{21}^2, B_0$ )	$\chi_{gl_{min}}^2/19d.o.f.$	$\chi_{rates}^2/1d.o.f.$	$\chi_{sp}^2/16d.o.f.$
1	$(7.1 \times 10^{-9} eV^2, 6.7 \times 10^4 G)$	9.94	0.100	9.79
2	$(1.32 \times 10^{-8} eV^2, 1.27 \times 10^5 G)$	11.83	0.290	11.33
3	$(1.25 \times 10^{-8} eV^2, 9.4 \times 10^4 G)$	9.81	0.116	9.63
4	$(1.67 \times 10^{-8} eV^2, 1.69 \times 10^5 G)$	12.7	0.708	10.95
5	$(2.13 \times 10^{-8} eV^2, 1.44 \times 10^5 G)$	11.88	0.133	11.82
6	$(1.78 \times 10^{-8} eV^2, 9.7 \times 10^4 G)$	12.29	0.366	11.83
7	$(1.45 \times 10^{-8} eV^2, 2.28 \times 10^5 G)$	12.0	0.764	10.16

Table V - Global fits: the values of  $\Delta m_{21}^2$  and  $B_0$  at the global best fit for each profile, the corresponding values of  $\chi_{rates}^2$  and  $\chi_{spectrum}^2$ .

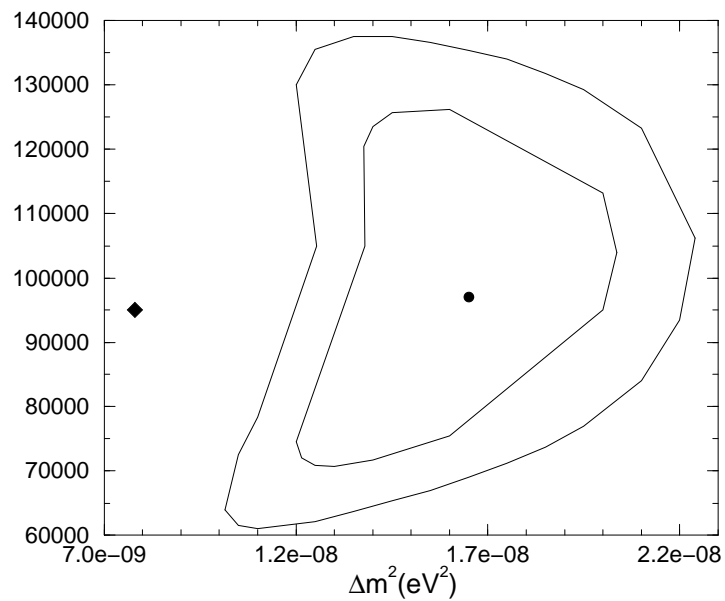
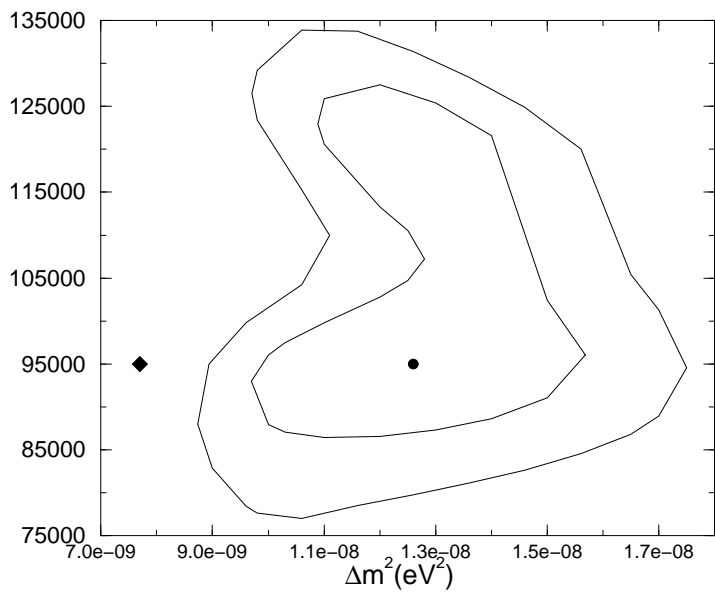
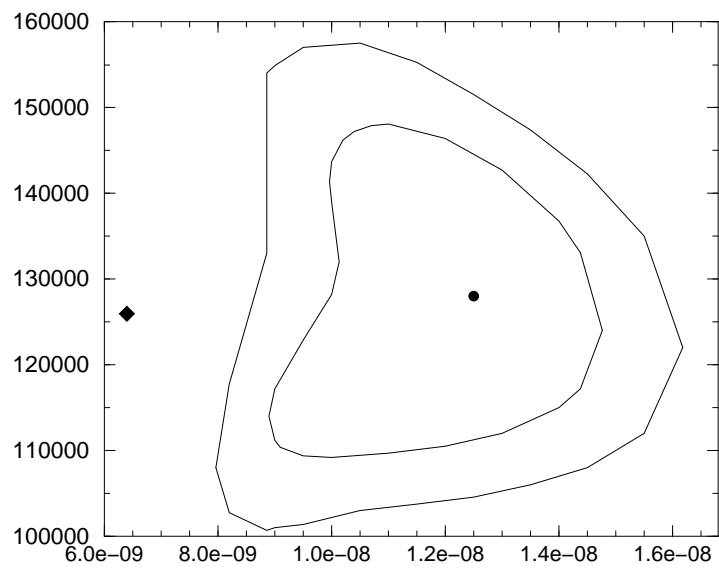
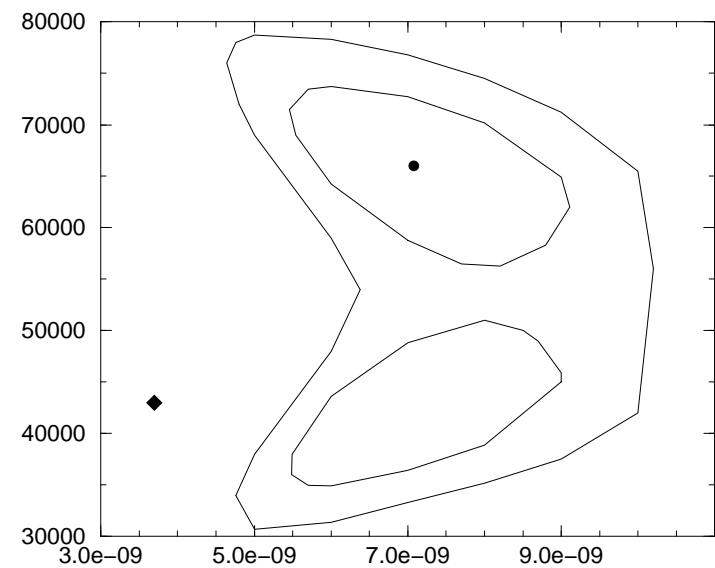
## Figure captions

Fig. 1. 90% and 99% CL regions with respect to rate best fits on the  $\Delta m_{21}^2$ ,  $B_0$  (peak field value) plane. Units are  $eV^2$  (x-axis) and Gauss (y-axis). From left to right and top to bottom: profiles 1, 2, 3, 6. Circles denote the rate best fits and diamonds the spectrum best fits (for the corresponding values of  $\chi^2$  see tables III and IV). The apparent mismatch between spectrum and rate best fits is statistically meaningless as can be seen from the last column of Table IV and the global fits (Table V).

Fig. 2. The electron recoil spectrum prediction for profile 1 for the values of  $\Delta m_{21}^2$ ,  $B_0$  corresponding to the rate best fit (table III) as a function of the total electron energy superimposed on the data set for 1117 days [2]. For this curve  $\chi_{sp}^2 = 9.85$  (see table III). Units are in eV. Notice the moderate rise in the theoretical curve for  $E_e \geq 12 MeV$  from the effect of hep neutrinos.

Fig. 3. Same as fig.2 for the values of  $\Delta m_{21}^2$ ,  $B_0$  corresponding to the spectrum best fit. For this curve  $\chi_{sp}^2 = 9.46$  (see table IV).

Fig. 1.



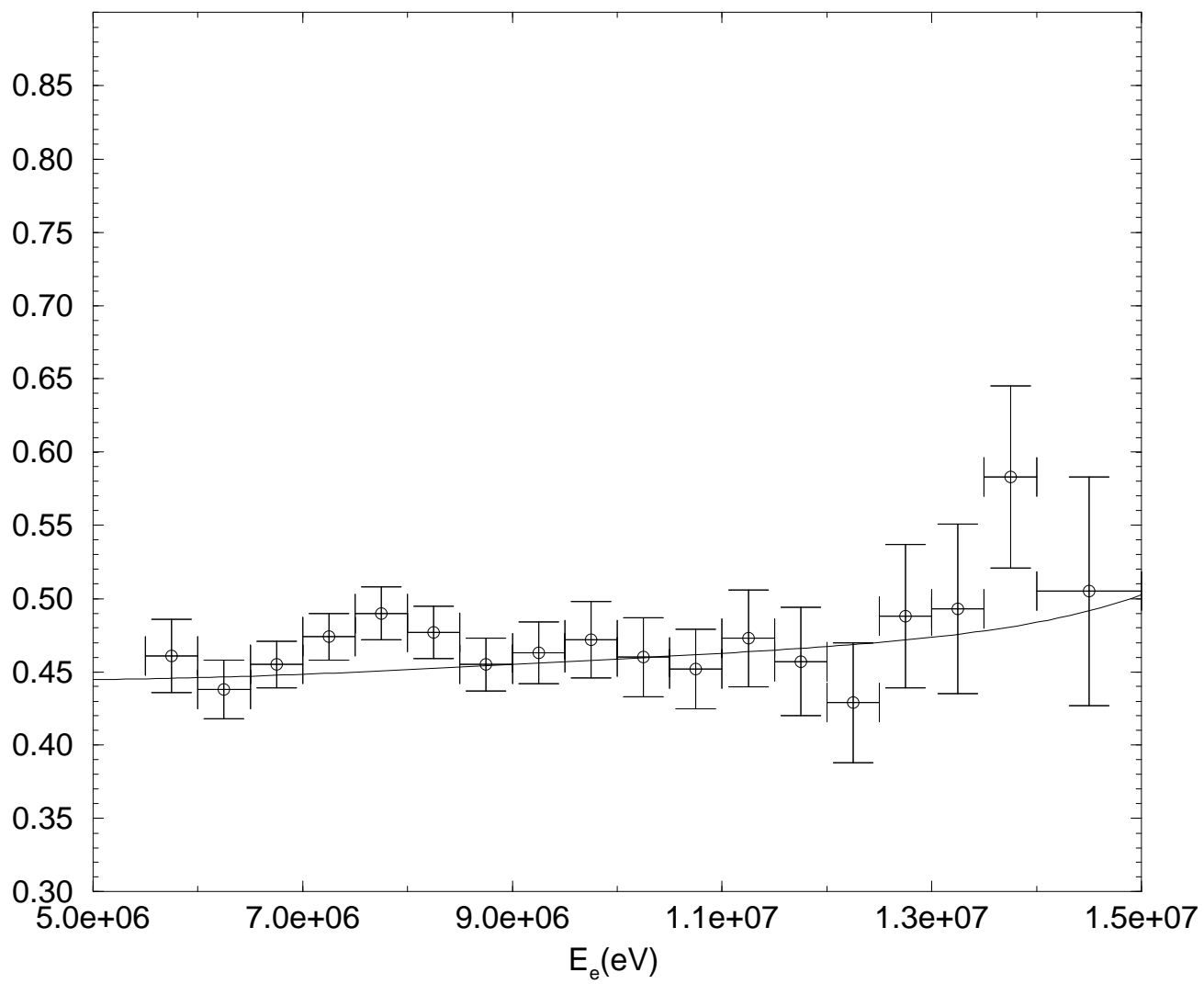


Fig. 2.

Fig. 3.

